Improvement of thermal and abrasion resistance performance of polyphenylene sulfide composite through 3-mercaptopropyl trimethoxysilane treatment of carbon fiber and graphene oxide fillers

Minsu Kim [a], Jooyoung Lee [a], Minhaeng Cho [d], Jooheon Kim [a,b,c,*]

[a] School of Chemical Engineering & Materials Science, Chung-Ang University, Seoul, 06974, Republic of Korea
[b] Department of Advanced Materials Engineering, Chung-Ang University, Anseong-si, Gyeonggi-do, 17546, Republic of Korea
[c] Department of Intelligent Energy and Industry, Graduate School, Chung-Ang University, Seoul, 06974, Republic of Korea
[d] School of Mechanical Engineering, Chung-Ang University, Seoul, 06974, Republic of Korea

ARTICLE INFO

ABSTRACT

The aim of this study was the improvement of the thermal conductivity and tribological properties of polyphenylene sulfide (PPS) with carbon fiber (CF) and graphene oxide (GO) fillers. Whereas CF reduce the mechanical strength of PPS, 3-mercaptopropyltrimethoxysilane (MPTMS)-treated CF improve the interfacial adhesion properties of fillers and PPS matrices, which increase the mechanical properties of composites. The improved thermal and mechanical properties of composites were confirmed via diffraction scanning calorimetry, dynamic mechanical analyzer, and wear test. The silane-modified PPS/20M-CF/5M-GO composite has a thermal conductivity of 0.323 W/m•K, which is 175% greater than that of the neat PPS composite. The friction coefficient has decreased from 0.236 to 0.176 and the specific wear rate has decreased from 1200 to 300 E−07 mm^3/N•m.

1. Introduction

Polymer materials have widely been used in different fields such as in the aerospace field [1,2], energy industry [3,4], textile industry [5], biology, medical science [6,7], and automotive industry [8,9]. Polymer materials have many advantages such as their low cost and light weight; in addition, they are easy to process and do not react with water. The performance of automobiles can be improved by reducing the weight of their components. Therefore, polymer plastics are used in various interior and exterior materials in the automotive industry. For instance, polycarbonate (PC) is a polymer plastic widely used for interior and exterior materials of automobiles [10,11]. More specifically, PC is used for headlamp lenses, outer door handle fields, wheel caps, roof rails, and bumpers [12,13]. However, the use of PC does not result in good chemical stability. By contrast, the use of polyamide (PA) results in good chemical stability, thermal stability, impact resistance, friction, and wear resistance. Hence, PA is used in engine room components, cylinder head covers, engine covers, cooling fans, and outdoor handles [14–16]. In addition, various polymer plastics such as acrylonitrile butadiene styrene copolymers, polybutylene terephthalate (PBT), polyurethane, polyvinyl chloride (PVC), polyethylene (PE), and polypropylene are used [17–21]. Among these plastic, polyphenylene sulfide (PPS) is a crystalline super engineering plastic with very high heat resistance, good chemical resistance, flame-retardancy properties, and dimensional stability [22]. The high heat deflection temperature (above 270 °C) makes PPS a suitable interior material that withstands high temperatures that occur, for instance, in engine rooms [23]. Because of its good wear resistance, many researchers are studying its suitability as a wear resistance material. D. Zhang et al. reported PPS composites with short carbon fiber, graphite, and tungsten disulfide to improve the tribological properties. The PPS/SCF/Gr/WS$_2$ composite shows low specific wear rate (3.57 E−07 mm^3/Nm) lubricated with diesel [24]. A. Jain et al. fabricated PPS composite with short carbon fibers, graphene oxide, nano diamonds as a filler. Under water lubricated condition, the wear rate was reduced in the order of 10^3 [25]. However, the thermal conductivity of PPS is only 0.2 W/mK which is lower than other engineering plastic such as PBT (0.27 W/mK) [18], PVC (0.45 W/mK) [19], PE (0.5 W/mK for high density PE) [20]. And PPS has a low glass temperature (near 90 °C) due to the flexible sulfide linkage between the aromatic rings and a low impact strength [25,26]. These drawbacks should be improved to applicate PPS composites for automotive industrial.

In this study, a highly wear-resistant PPS matrix was combined with

---

carbon fiber (CF) and graphene oxide (GO) fillers to improve the tribological and thermal properties. Carbon fibers have a low density, good chemical resistance, and high strength [27]. K. Stoeffler et al. reported PPS composites reinforced with recycled carbon fiber. The mechanical properties was enhanced with adding recycled carbon fiber fillers [28]. S. Zhou et al. reported PA6/PPS matrix with 15 wt% carbon fiber which enhanced mechanical and tribological properties [29]. GO has been widely used as a filler to improve the mechanical and tribological properties of polymer matrices such as Nylon and PPS [30]. By adding silane-treated carbon fibers and graphene oxide to the PPS matrix, the tribological performance can be improved. The PPS/CF/GO composite was prepared via melt extrusion. By modifying the carbon fiber and GO fillers with silane material, the mechanical and thermal properties of the composites were improved. 3-mercaptopropyl trimethoxysilane (MPTMS) is a silane coupling agent with a thiol group (R–SH). The thiol functional group in MPTMS can form hydrogen bonding with the sulfur of PPS. Treating the CF and GO fillers with MPTMS to improve the interfacial adhesion with the PPS polymer matrix could improve the thermal and tribological properties of the PPS/CF/GO composites. Before the MPTMS treatment, the CF fillers were pretreated with acid and strong oxidizer to form hydroxyl group on the surface of CF. Whether or not MPTMS was combined with the CF and GO fillers was confirmed through Fourier-Transform Infrared spectroscopy, Thermogravimetric analysis and X-ray photoelectron spectroscopy, and it was confirmed that the CF filler was aligned in a certain direction in the PPS matrix through MPTMS treatment. The storage modulus of the composite PPS/20M-CF/5M-GO was enhanced 2 times compared to neat PPS. The thermal conductivity was increased to 0.323W/mK which is 175% greater than neat PPS. In addition, certain tribological properties such as the friction coefficient and specific wear rate were improved. The friction coefficient was decreased due to the addition of silane treated carbon fiber and GO. Hence, these PPS/CF/GO composites can be used in interior or exterior materials and heat pumps in the automotive industry.

2. Experimental section

2.1. Materials

Polyphenylene sulfide (PPS) was obtained from Solvay, and the graphene oxide power was purchased from Grapheneall (Korea). The chopped carbon fiber powder was purchased from FRP shop (Korea). Moreover, methyl alcohol (99%), nitric acid (60%), and tetrahydrofuran (THF) were purchased from Daejung Chemical and Metals Co., Ltd. (Seoul, Korea), and 3-mercaptopropyl trimethoxysilane (MPTMS, 95%) and 1.0 M lithium aluminum hydride in THF (LiAlH$_4$) solution were obtained from Sigma-Aldrich. All reactants were used as received without purification.

2.2. Treatment of carbon fibers and graphene oxide

The 10 g of chopped carbon fiber powder was treated with nitric acid refluxing at 120 °C for 6 h to promote surface oxidation and subsequently dried in a vacuum oven at 60 °C overnight. The obtained carbon fibers were treated with LiAlH$_4$ solution in THF solvent for 24 h and dried in a vacuum oven at 60 °C overnight. Subsequently, the 10 g of oxidized carbon fibers were dispersed in methyl alcohol; 3 g of MPTMS was slowly dropped into the solution, which was then stirred for 24 h. The obtained MPTMS-treated carbon fibers are called "M-CF".

The graphene oxide was directly treated with MPTMS owing to the oxygen-functional groups on the surfaces. The 5 g of graphene oxide powder was dispersed in 60 ml methyl alcohol; subsequently, 1.5 g of MPTMS was added to the solution, which was then stirred for 24 h. The obtained MPTMS-treated graphene oxides are called "M-GO"

Table 1
Component ratios of composites.

Sample	PPS (%)	CF (%)	M-CF (%)	GO (%)	M-GO (%)
Neat PPS	100				
PPS/20CF	80	20			
PPS/30CF	70	30			
PPS/40CF	60	40			
PPS/20M-CF	80		20		
PPS/20M-CF/5GO	75		20	5	
PPS/20M-CF/5M-GO	75		20		5

2.3. Fabrication of PPS/CF/GO composite

The untreated and MPTMS-treated carbon fibers and GO and neat PPS were inserted into a twin-screw melt extruder (model BA-11, Bautek, Korea) operating at 270–300 °C. During extrusion, the vacuum pump was operated to extract vaporized gases and moisture from the extruder screw zones. The extrudates were collected and pelletized at 290 °C via injection molding (model BA-915, Bautek, Korea) to prepare composites. The component ratios are shown in Table 1.

2.4. Characterization

Fourier-transform infrared (FT-IR) spectroscopy (PerkinElmer Spectrum One) was used to confirm the successful attachment of MPTMS on the carbon fiber and graphene oxide surfaces. The binding energies of the carbon fiber and GO fillers were determined via X-ray photoelectron spectroscopy (XPS; K-Alpha, Thermo UK) with a 1486.6 eV Al K$_\alpha$ X-ray source. The chemical structures in the fillers were determined with a Raman spectrometer II (DXR2xi, Thermo) with a near-infrared laser operating at 532 nm and a CCD detector. In addition, the crystalline structures of the fillers were determined via X-ray diffraction (XRD; D8 Advance, AXS Bruker) over a 2θ range of 10°–80° at 40 kV and 40 mA and a scan rate of 1° s^{-1} under λ = 0.154056 nm Cu K$_\alpha$ radiation. Moreover, field-emission scanning electron microscopy (FE-SEM; SIGMA) was used to study the morphology of the GO and CF fillers and cross-sectional images of the fabricated composites. The elemental maps of M-GO were prepared with energy-dispersive X-ray spectroscopy (EDS; Thermo NORAN System 7, SIGMA). The elemental maps and morphology of M-CF were prepared with field-emission transmission electron microscopy (FE-TEM; JEM-F200). Thermogravimetric analysis (TGA, TGA-2050, TA Instruments) of the untreated and MPTMS-treated fillers was performed by heating the samples from room temperature to 800 °C at 20 °C min^{-1} in a nitrogen atmosphere. The crystallization characteristics versus the temperature of the untreated and MPTMS-treated fillers were determined with differential scanning calorimetry (DSC, DSC-Evo, KEP Tech). The thermal conductivity (κ) was calculated based on the relationship $\kappa = \alpha\%\rho\%C_p$, where ρ, α, and C_p are the composite density, thermal diffusivity, and specific heat capacity, respectively. Furthermore, the LFA 447 Nanoflash (NETZSCH) equipment was used to measure the thermal diffusivity, and DSC was used to quantify the specific heat capacity of the fabricated composites. The densities of the composites were calculated with the Archimedes method. Their mechanical properties were measured with a universal testing machine (3344Q9465, Instron Co.) at a cross-head speed rate of 1 mm/min. The viscoelastic properties of the composites were determined at −20 to 300 °C with a dynamic mechanical analyzer (DMA; Triton Technologies, UK). The wear test was conducted with the ball-on-disk method and multi-purpose wear simulation system (NEO-TRIBO). In this step, the composites were injected into a mold with 30 mm diameter and 4 mm thickness. The counterpart ball was SUJ2 bearing steel, the ball diameter was 12.7 mm, the rotation radius was 11.5 mm, the load applied to the sliding part was 10 N, and the sliding speed was 83 rpm for 2 h. Finally, the wear test was conducted in the dry state without oil on the surface.
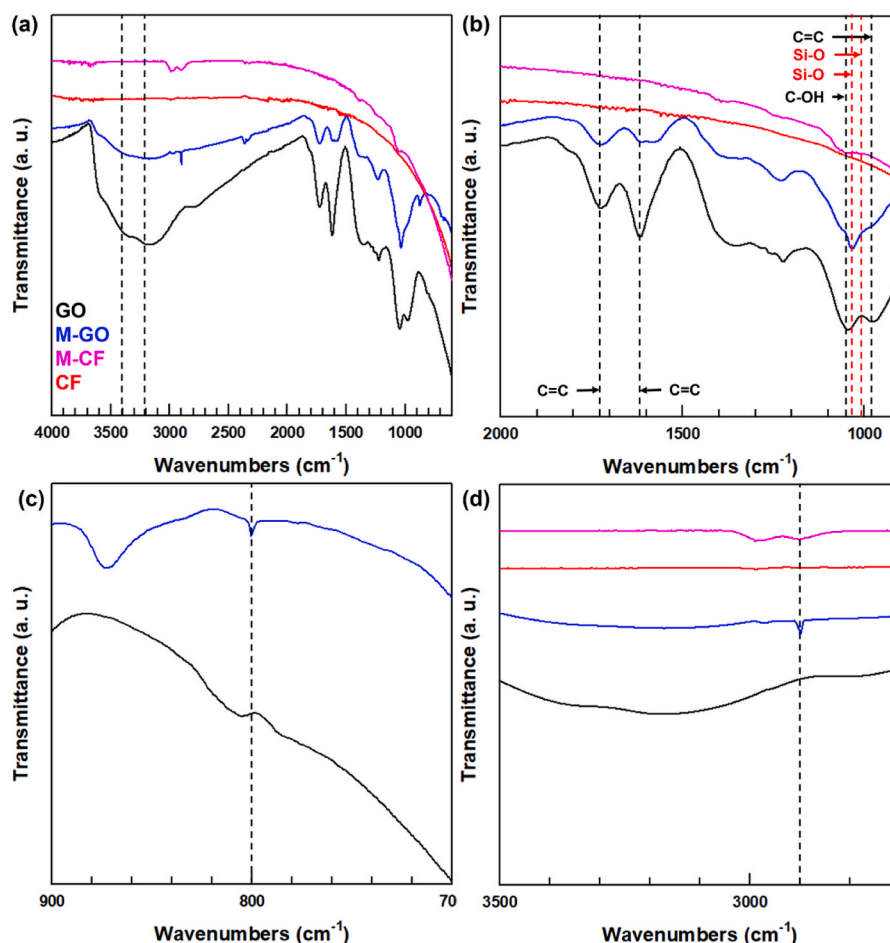
Fig. 1. (a) FT-IR spectrum and the corresponding high-resolution FT-IR spectra with the wavenumber (b) from 2000 to 900 cm^{-1} (c) from 900 to 70 cm^{-1} and (d) from 3500 to 2700 cm^{-1} of GO, M-GO, CF and M-CF fillers.

3. Results and discussion

3.1. Confirmation of successful MPTMS attachment on carbon fiber and graphene oxide fillers

To confirm the successful attachment of MPTMS on the carbon fiber and GO, the samples were studied with FT-IR spectroscopy as shown in Fig. 1. The pristine carbon fibers exhibit straight lines from 4000 to 2000 cm^{-1}, which decrease rapidly. After the attachment of MPTMS on the carbon fibers, two small peaks occur near 2900 cm^{-1}, which correspond to –OH functional groups and methyl group of MPTMS; the small peak at 1050 cm^{-1} is associated with Si–O bonds that originate from MPTMS [31]. From the FT-IR results, it was difficult to find the FT-IR peak of MPTMS because it was less attached to the surface of the carbon fiber (about 10%) as shown TGA result in Fig. 5(a), will be discussed below. The pristine GO shows a wide peak from 3680 to 1860 cm^{-1}, which correspond to –OH functional groups on the GO surfaces. The FT-IR peaks at 1720, 1617, 1048, and 970 cm^{-1} are associated with C=O, C=C, C–OH, and C=C bonds, respectively [31]. After the attachment of the MPTMS on the GO, the wide peak between 3680 and 1860 cm-1 decreased because MPTMS reacts with the –OH functional groups of the GO surface. and the small peak of 2900 cm^{-1} shows the methyl and methylene groups of MPTMS. The M-GO sample still shows 1735, 1650, and 1052 cm^{-1} peaks, which correspond to pristine GO. The three additional peaks at 1035, 1000 (which correspond to Si–O–Si bonds) and 800 cm^{-1} (stretching vibration peak of Si–O bond) confirm the successful attachment of MPTMS on the GO surface. The MPTMS attachment on carbon fibers and GO can also be confirmed via XPS, TGA,

and XRD analyses and Raman spectra.

Fig. 2 shows the XPS results of the GO and M-GO samples. The C 1s peak of pristine GO comprises five peaks at 289.4, 288.24, 286.79, 284.74, and 285.66 eV, which correspond to O–C=O, C=O, C–O–C, C–C, and C–OH bonds, respectively [31]. The C–OH peak at 285.66 eV vanished, whereas S 2p peaks of thiol functional groups (R–SH) emerged at 164.79 and 163.58 eV after the MPTMS treatment. The Si 2p peak at 102 eV indicated Si–O bond in MPTMS. Thus, the MPTMS molecules react with –OH functional groups on the GO surfaces. The carbon fibers show a similar C 1s peak, which is related to C=O, Si–O–C, C–S, and C–C bonds due to the surface oxidation of the carbon fibers, Si–O–C bonds of MPTMS, C–S bonds of MPTMS, and C–C bonds of the carbon fibers, respectively, as shown in Fig. 2(e and f) [32]. Similar to M-GO, M-CF also shows S 2p peak of R–SH thiol group and Si 2p peak of Si–O bond in MPTMS. Evidently, MPTMS has successfully been attached to the carbon fiber surfaces.

The Raman spectra were recorded to confirm the change in the surface defects of the carbon fibers and GO before and after the MPTMS treatment as shown in Fig. 3(a). The change in the surface defects can be confirmed based on the calculated ID/IG ratio of the D and G bands. Pristine GO has an ID/IG ratio of 1.22, which decreases to 1.08 for M-GO. The ID/IG ratio has decreased owing to the defects on the GO surface during the MPTMS treatment. A similar trend occurred during the MPTMS treatment of the carbon fibers. The ID/IG ratio of the untreated carbon fibers is 1.38. After the MPTMS treatment, the ID/IG ratio decreased to 1.31 for M-CF. Before the MPTMS treatment, the carbon fibers were treated with nitric acid and LiAlH$_4$ to obtain oxygen-containing functional groups, which have resulted in defects on the
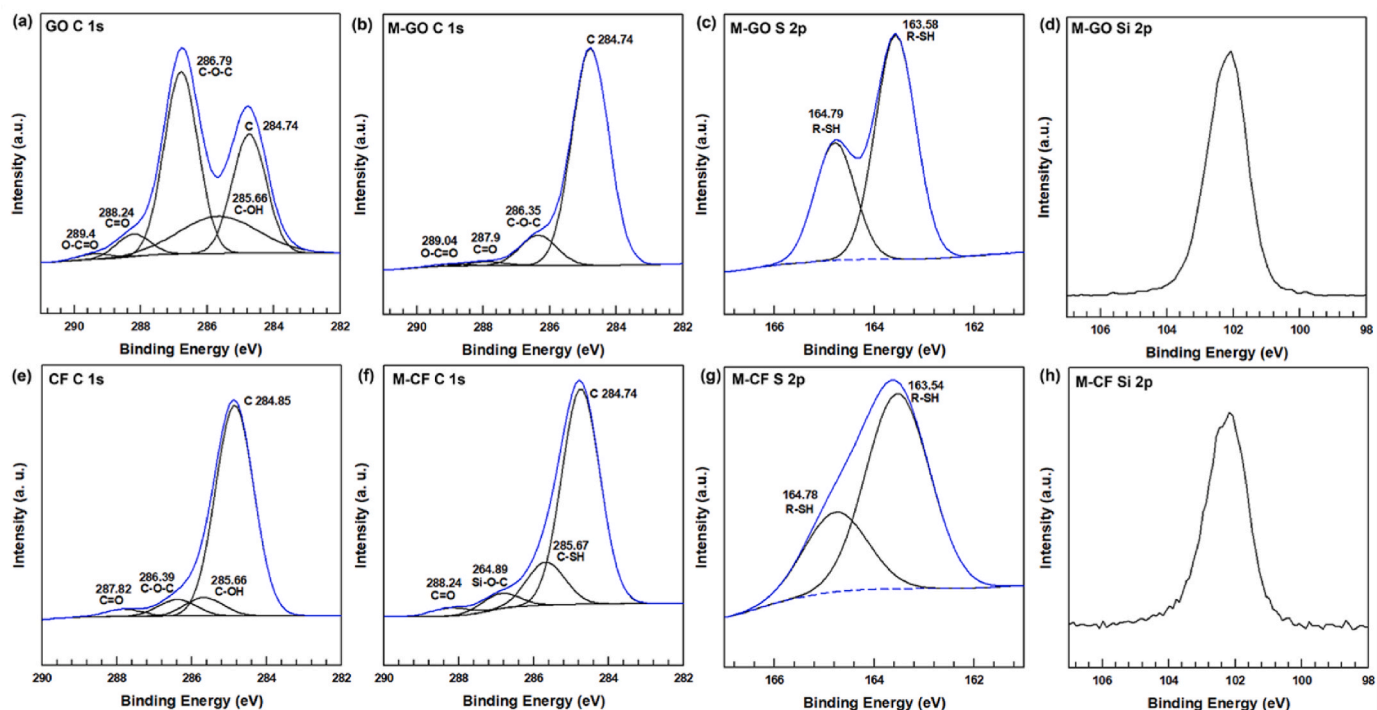
Fig. 2. High-resolution XPS spectra of (a) GO C 1s peaks, and M-GO (b) C 1s peaks (c) S 2p peak (d) Si 2p peak. High-resolution XPS spectra of (e) CF C 1s peaks, and M-CF (f) C 1s peaks (g) S 2p and (h) Si 2p peaks.
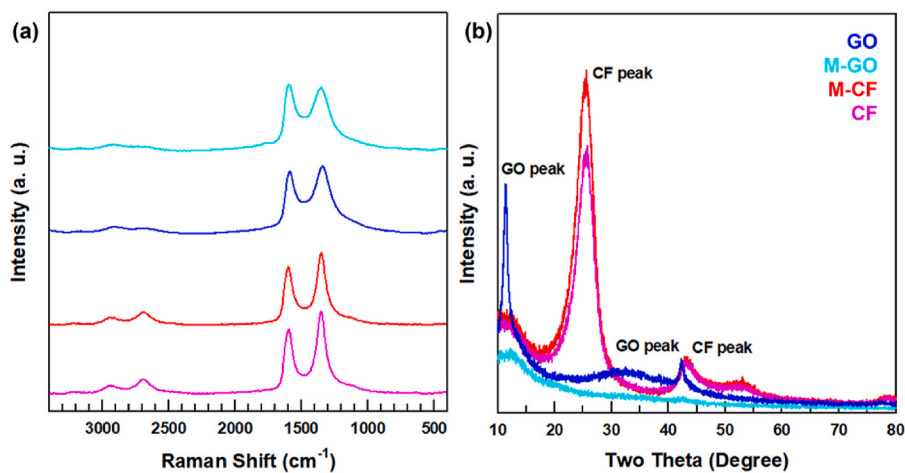

Fig. 3. (a) Raman spectra (b) XRD patterns of GO, M-GO, CF and M-CF fillers.

carbon fiber surfaces.

The crystallinity of the fillers was studied with XRD spectroscopy as shown in Fig. 3(b). The pristine GO shows two specific peaks at 11° and 42°, which agree well with those reported in Ref. [33]. After the MPTMS treatment, the peak at 11° decreased and became broad; by contrast, the other peak at 42° vanished. Thus, the MPTMS was successfully attached to the GO surface, and the GO sheets were exfoliated, which has reduced the GO crystallinity. In the case of the carbon fibers, the peak at 25° to 26° decreased after the MPTMS treatment (such as that of M-GO). Unlike the M-GO sample, the carbon fibers exhibit high crystallinity before and after the MPTMS treatment. According to the XPS, FT-IR, Raman, and XRD analysis results, MPTMS has been successfully attached to the carbon fibers and GO; in addition, the MPTMS–CF–GO components are well connected after the treatment.

3.2. Morphologies of carbon fiber and GO fillers

The morphologies of the carbon fiber and GO fillers were determined with FE-SEM images (Fig. 4). The MPTMS-treated carbon fiber has a clear surface with a diameter of 10 μm. The MPTMS treatment has not changed its morphology. To confirm the successful attachment of MPTMS, EDS elemental maps were recorded using FE-TEM due to the less attachment of MPTMS on carbon fiber surface. The presence S and Si atoms of MPTMS is confirmed that MPTMS was successfully attached to carbon fiber surface. Unlike the M-CF sample, M-GO has clearer EDS elemental maps obtained from FE-SEM owing to the higher ratio of MPTMS, which is confirmed by the TGA results.

3.3. Thermal properties of carbon fiber and graphene oxide fillers

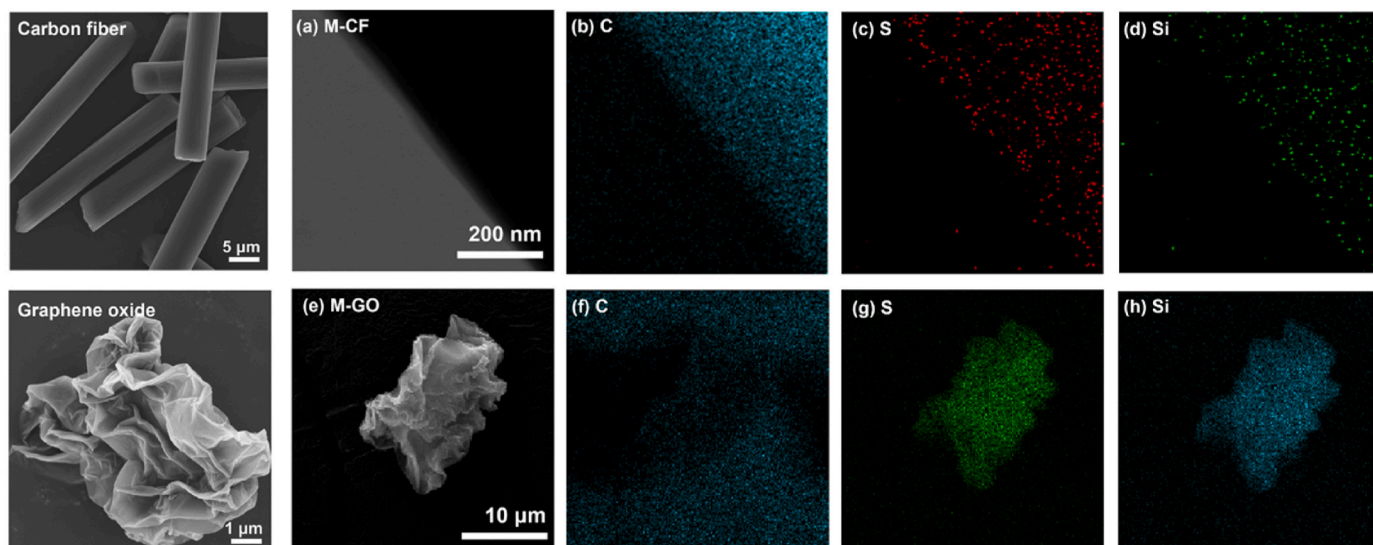The TGA analysis was conducted in nitrogen (N₂) gas. The untreated

Fig. 4. (a) FE-TEM image, EDS elemental mappings of (b) carbon (C) (c) sulfur (S) (d) silicon (Si) of M-CF filler. (e) FE-SEM image, EDS elemental mapping of (f) C (g) S and (h) Si of M-GO filler. (For interpretation of the references to colour in this figure legend, the reader is referred to the Web version of this article.)
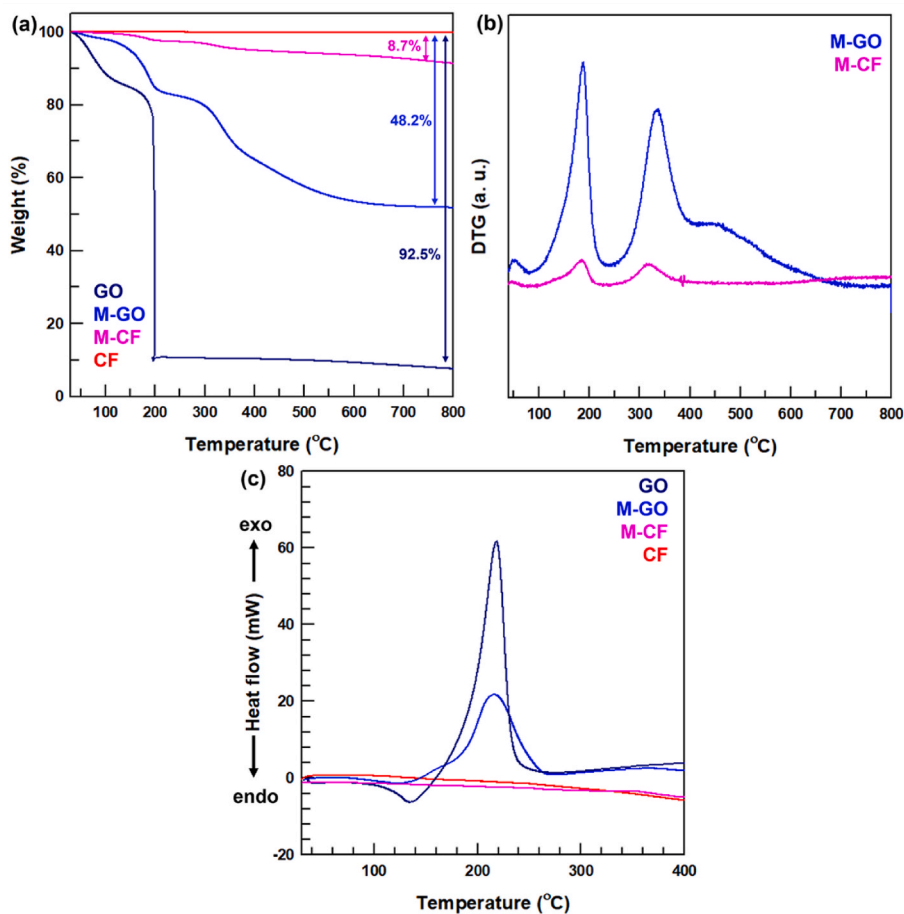

Fig. 5. (a) TGA curves. (b) TGA derivative (c) DSC curves of GO, M-GO, CF and M-CF fillers.

carbon fibers are stable in N_2 gas up to 800 °C, whereas GO shows two parts of thermal degradation as shown in Fig. 5(a). The weight loss up to 150 °C is due to the removal of water molecules trapped between the GO sheets. Above 150 °C, oxygen-containing functional groups are pyrolyzed. After 200 °C, 10% of the GO weight remains. Due to the TGA analysis was conducted in a nitrogen atmosphere, carbon atoms in GO

partially reacted with oxygen in the hydroxyl groups attached to the GO surfaces, leaving 10% by weight. The TGA plot of M-GO shows a similar thermal degradation behavior of GO and the weight loss decreases above 200 °C, which is similar to the behavior of previously reported MPTMS-treated materials. The MPTMS-treated carbon fibers reveal slight thermal degradation above 350 °C. Moreover, the M-GO sample is slightly
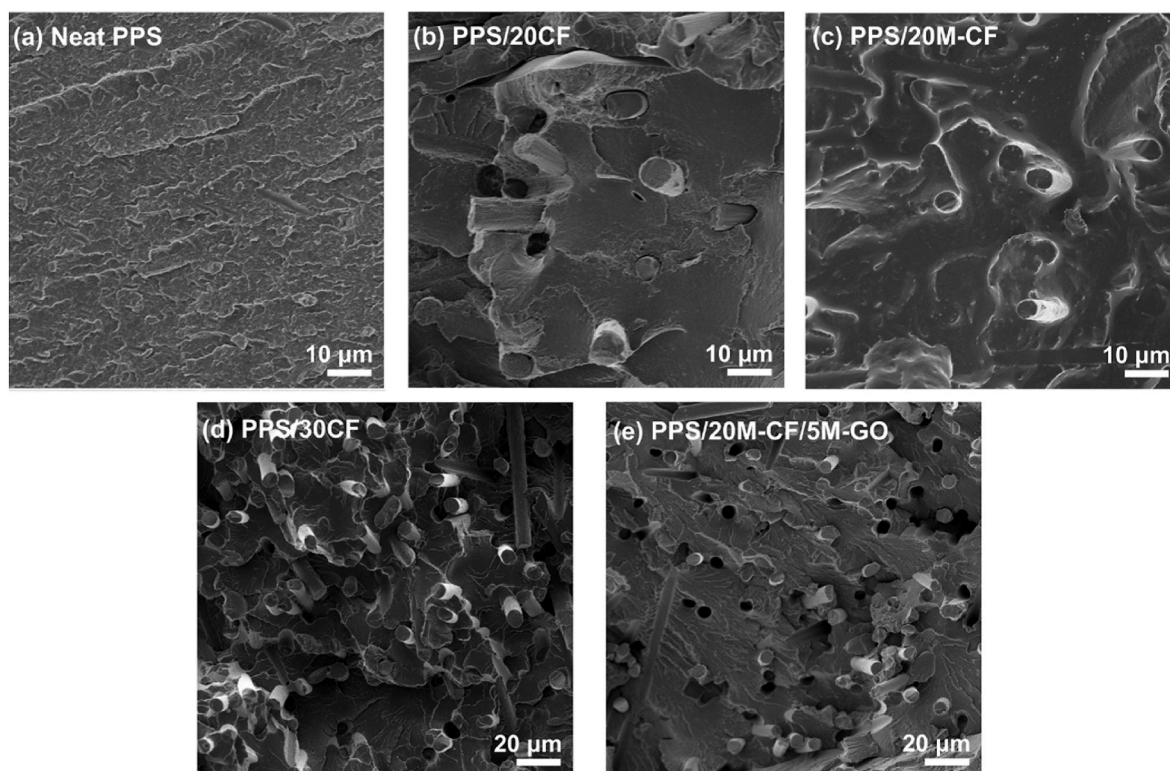
Fig. 6. Cross-sectional FE-SEM images of (a) neat PPS (b) PPS/20CF (c) PPS/20M-CF (d) PPS/30CF and (e) PPS/20M-CF/5M-GO composites.

thermally degraded above 350 °C, which indicates the degradation of MPTMS above 350 °C [34,35]. The weight loss of M-GO after TGA method was 48.2% while weight loss of GO was 92.5% which indicates about 44% of MPTMS was attached on the surface of GO. Similar to M-GO, M-CF shows similar trend during TGA analysis. The weight loss of M-CF was only 8.7% which indicates 8.7% of MPTMS was attached on carbon fiber. The carbon fiber is a material with strong chemical resistance. Therefore, a very small amount of hydroxyl groups were formed on the carbon fiber surface through acid and LiAlH$_4$ treatment. For this reason, only 8.7% of MPTMS was attached on the carbon fiber which makes difficult to find peaks related to MPTMS in the FT-IR analyzed above (Fig. 1).

The DSC curve of GO in Fig. 5(c) shows endothermic heat flow up to 150 °C, which then becomes endothermic heat flow above 150 °C. Under 150 °C, the trapped water molecules between the GO sheets evaporate; above 150 °C, the oxygen-containing functional groups are pyrolyzed. Because the pristine GO was not subjected to a purification process, the exothermic peak is stronger than that of the M-GO filler. After the attachment of MPTMS on the GO surface, the product was dried in a vacuum oven overnight, which has resulted in a lower weight loss in the TGA results and a smaller exothermic peak in the DSC curve. The DSC curves of the untreated carbon fibers and M-CF show approximately straight lines because the carbon fibers remain stable at high temperatures, as presented in the TGA results.

3.4. Cross-sectional morphologies of PPS/carbon fiber/graphene oxide composites

The FE-SEM study was conducted to determine the cross-sectional morphologies of the composites as shown in Fig. 6. The FE-SEM image of the neat PPS shows an amorphous and unclear surface. The composite with untreated carbon fibers has randomly distributed-fibers without a specific filler orientation. After the MPTMS treatment, the M-CF filler is ordered with a specific direction; this can be due to the attached MPTMS. Compared to the untreated carbon fiber composite, the

MPTMS-treated carbon fiber composite shows fewer cracks and voids and a smooth surface. This can affect the mechanical properties of the composite, as discussed below. After the addition of graphene oxide, the morphology of the composite does not look different.

3.5. Thermal and mechanical properties of PPS/carbon fiber/graphene oxide composites

The measured through-plane thermal diffusivity and conductivity of the carbon fiber and GO fillers in the PPS matrix composites are shown in Fig. 7. The thermal diffusivity has been increased up to 30% carbon fiber content (PPS/30CF), while decreased when the carbon fiber content was 40% (PPS/40CF). As the carbon fiber content increases, agglomeration of the carbon fiber appears in the PPS composite and the interface between carbon fiber and PPS matrix increases, which can become factors hindering thermal diffusivity in the through-plane direction. After the MPTMS treatment, the carbon fiber fillers are aligned with a specific direction; by contrast, the untreated carbon fiber composite exhibits no specific direction, as discussed above (Fig. 6). Moreover, the MPTMS-treated carbon fibers and PPS matrix have greater bonding strength owing to the thiol functional groups of MPTMS; these decrease the thermal resistance at the interface and increase thermal conductivity. The thermal conductivity was calculated by multiplying the thermal diffusivity, density, and specific heat capacity. The obtained thermal conductivities are presented in Fig. 7(b). The thermal conductivity increases with increasing carbon fiber content. In Fig. 6, the carbon fiber filler is randomly distributed and functions as a heat path. After the MPTMS treatment, the carbon fiber filler is ordered with a specific direction, and the thermal conductivity is increased. The highest thermal conductivity of the PPS/20-M-CF/5-M-GO composite is 0.323 W/m•K (for comparison, the thermal conductivity of neat PPS is 0.185).

The mechanical properties of the filler-reinforced polymer composites are determined by the compatibility and interfacial adhesion characteristics of the components and the dispersion characteristics of the filler. The tensile strength of neat PPS without a filler is 58 MPa, while
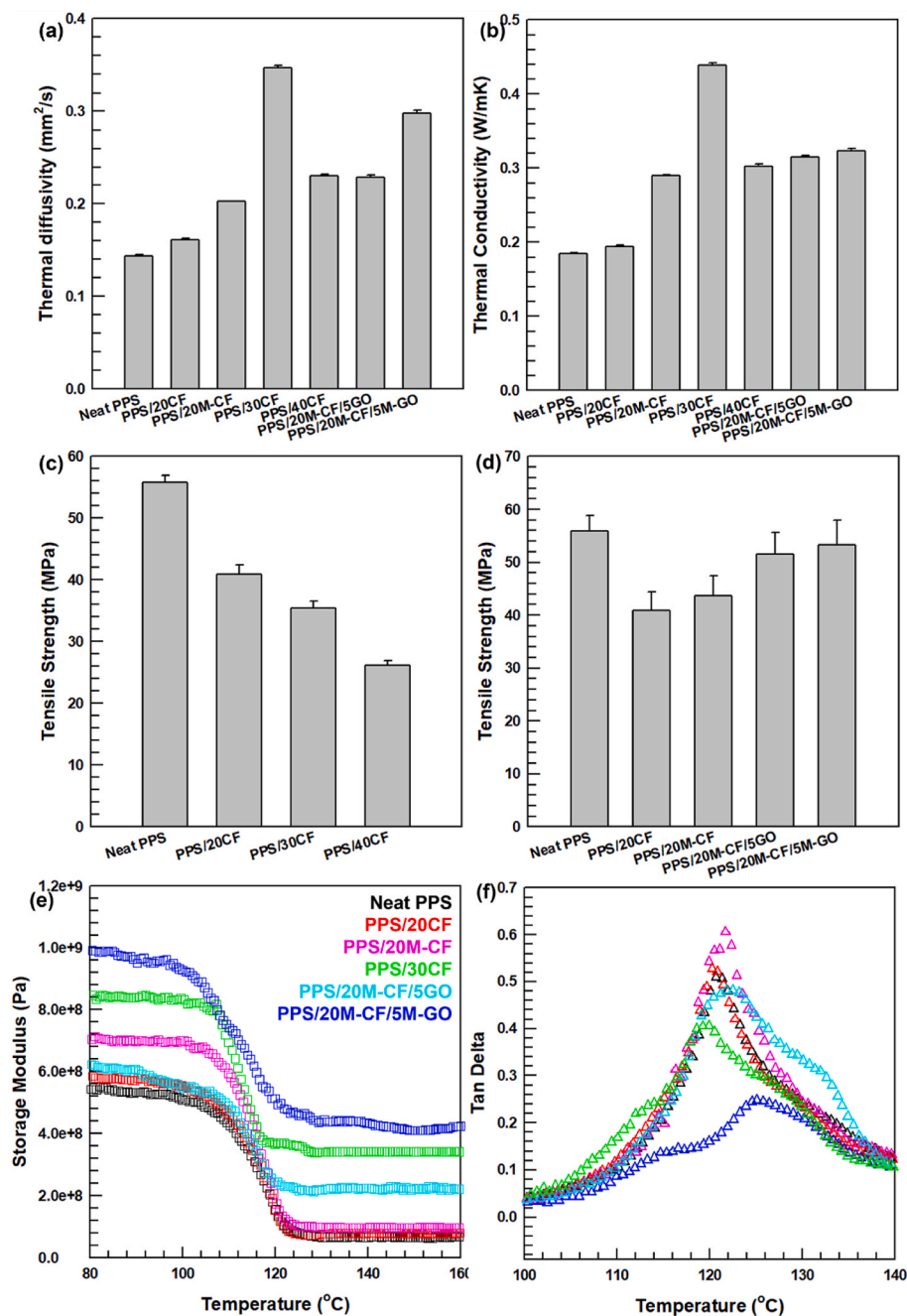
Fig. 7. (a) Thermal diffusivity (b) thermal conductivity of PPS/CF/GO composites. PPS/CF/GO tensile stress of (c) various carbon fiber ratio (d) MPTMS treatment. (e) Storage modulus and (f) tan delta of PPS/CF/GO composites.

the 20%, 30% and 40% PPS/CF composites have lower tensile strengths: 41, 35, and 26 MPa, respectively. Carbon fibers are known to have very high tensile strength (270 GPa [36]). However, in this study, the carbon fibers were chopped, which decreased their tensile strength. As the carbon fiber content increases, the tensile stress gradually decreases, as shown in Fig. 7(c). To maintain the good mechanical properties, we chose 20% carbon fiber content and studied the MPTMS-treated composite. When the carbon fibers are oxidized, the carbon fiber surface includes defects, which degrade the tensile strength of the composite. The MPTMS treatment has increased the tensile strength of PPS/20-M-CF to 51 MPa. Moreover, the addition of M-GO (i.e., the sample PPS/M-CF/M-GO) has increased the tensile strength (53 MPa, which is comparable to that of the neat PPS composite). The mechanical properties have been improved by adding MPTMS-treated carbon fibers

and GO to the composites; this was confirmed with the DMA as shown in Fig. 7(e and f). Owing to the introduction of carbon fibers on the PPS matrix, the glass transition temperature of the PPS composites has increased by increasing carbon fiber fillers (from 120.8 to 134.16 °C) due to the carbon fiber. Compared to PPS/20-CF composite, PPS/20-M-CF composite shows lower glass transition temperature, 121.53 to 120.27 °C. It can be seen that MPTMS treatment increases the bonding force between carbon fiber and PPS matrix and improved dispersibility of carbon fiber filler as discussed above (Fig. 6), which decreases glass transition temperature. Similar trend was shown in PPS/20-M-CF/5-M-GO composite which has 119.80 °C lower than PPS/20-M-CF/5-GO composite, 121.82 °C. Moreover, the storage modulus has increased owing to the introduction of carbon fibers and MPTMS treatment. This improvement is due to the improved stress
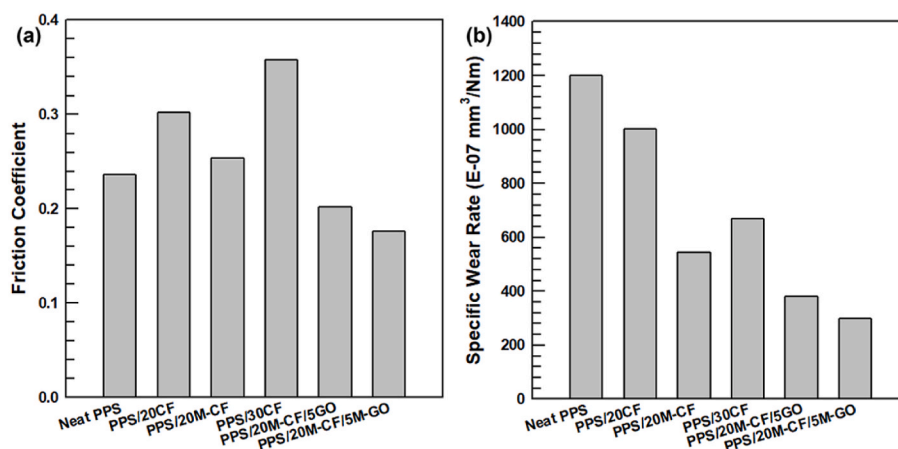
Fig. 8. (a) Friction coefficient and (b) specific wear rate of PPS/CF/GO composites with various filler ratio.
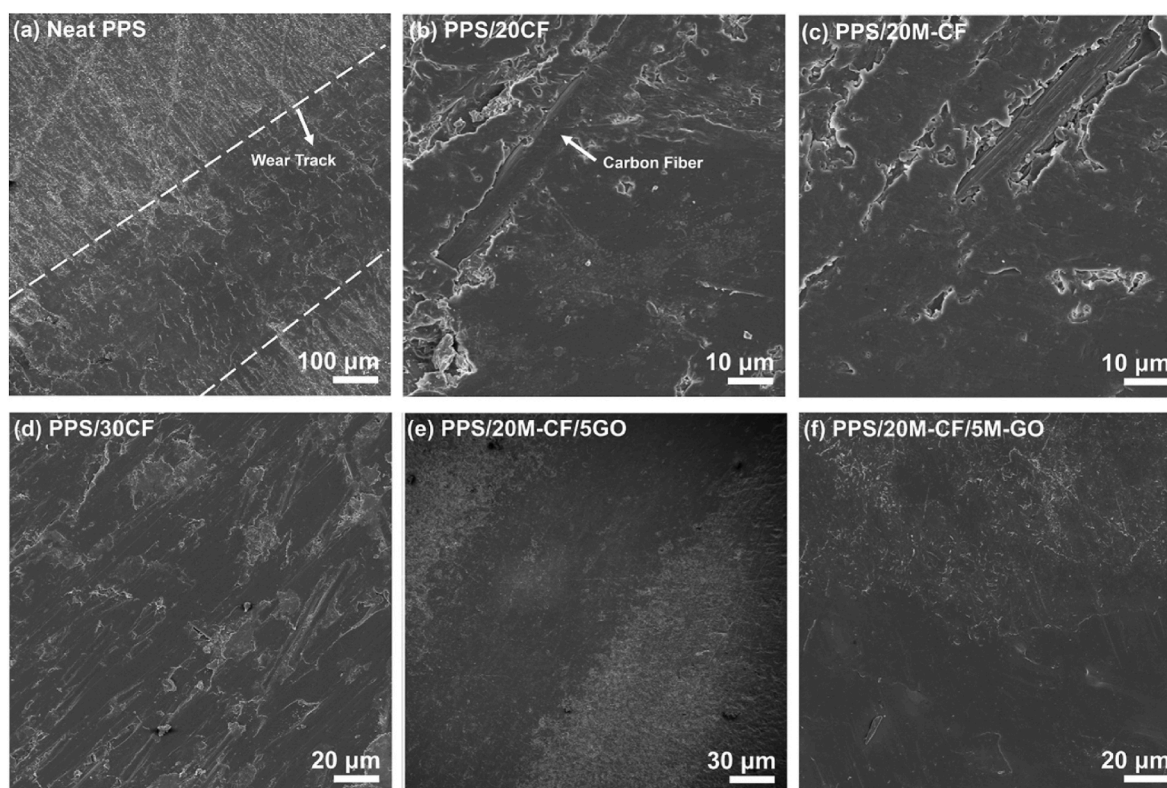

Fig. 9. FE-SEM images of (a) neat PPS (b) PPS/20CF (c) PPS/20M-CF (d) PPS/30CF (e) PPS/20M-CF/5GO and (f) PPS/20M-CF/5M-GO composites after wear test.

transfer at the interface of the composites. The MPTMS-treated composites have decreased voids and cracks, as shown in Fig. 4; they indicate improved stress transfer. The tensile strain of the 20% and 30% carbon fiber composites has increased, whereas the tensile strain of the 40% carbon fiber composite is decreased compared to that of the neat PPS composite. The carbon fibers are longer than 20 μm; this long length can keep the PPS matrix in place and increase the tensile strain. The MPTMS treatment has increased the bonding force between the PPS matrix and carbon fiber filler, thereby resulting in higher tensile strain.

Furthermore, wear tests were conducted to determine the tribological properties of the composites as shown in Fig. 8. The friction coefficient firstly increased from 0.236 to 0.402 for the neat PPS composite and to for the 40% carbon fiber-containing composite. The untreated carbon fiber-containing composites have some voids and cracks which increase the surface roughness, so it seems that the friction coefficient

was increased. After the MPTMS treatment for 20% carbon fiber-containing composite, the friction coefficient decreased to 0.254, and for 20% carbon fiber and 5% GO containing composite, the friction coefficient decreased to 0.176 which is 75% lower than the friction coefficient of neat PPS, 0.236. As shown in Figs. 6 and 9, the voids and cracks were diminished after MPTMS treatment, the friction coefficient was decreased compared to untreated composites. The top surface of the PPS/CF/GO was the smoothest in the MPTMS-treated samples for both CF and GO (PPS/20M-CF/5M-GO) as shown in Fig. 9(f). Due to the existence of hydroxyl group on GO surface and large surface area, good mechanical interlocking occurring on the corrugated rough surface of GO will lead to good interfacial adhesion between GO and PPS matrix [37]. In addition, treating with MPTMS on GO surface formed additional thiol functional group which can lead to good interfacial adhesion between GO and PPS. For this reason, the tribological performance was

Table 2
Physical properties before and after the wear test of the PPS/CF/GO composites.

Sample	Density (g/cm^3)	Before weight (g)	After weight (g)	Weight difference (g)	Applied load (N)	Sliding distance (m)
Neat PPS	1.208 ± 0.08	3.3731	3.3720	0.0011	10 N	720 m
PPS/20CF	1.357 ± 0.05	3.3746	3.3736	0.0010		
PPS/30CF	1.371 ± 0.07	3.4967	3.4962	0.0005		
PPS/40CF	1.405 ± 0.04	3.6373	3.6364	0.0009		
PPS/20M-CF	1.388 ± 0.08	3.7481	3.7472	0.0009		
PPS/20M-CF/5GO	1.396 ± 0.07	3.5830	3.5826	0.0004		
PPS/20M-CF/5M-GO	1.341 ± 0.05	3.5502	3.5499	0.0003		

Table 3
Comparison of specific wear rate of PPS/20M-CF/5M-GO composite with previously reported PPS composites.

Composite	Specific wear rate (E−05 mm^3/Nm)	Testing condition	Ref
PPS/10SCF	5	Dry	[25]
PPS/0.9 wt%CNT	1.838	Dry	[38]
PPS/PTFE/SCF20	3.79	Dry	[39]
PPS/PTFE/CF	4.28	Dry	[40]
PPS/0.47Ag	6.94	Dry	[41]
PPS@PDA-CNTs-SiC	2.5	Dry	[42]
PPS/20M-CF/5M-GO	3	Dry	This work

improved along with the improvement of the mechanical and thermal performances discussed above. The specific wear rate (W_s) was calculated with the equation below:

$$W_s = wear\ loss/D \times F \times L$$

where, D, F, and L denote the density of the composite, applied load and sliding distance, respectively. The physical parameters for calculating specific wear rate were shown in Table 2. The specific wear rate decreased from 1200 to 670 E−07 mm^3/N•m with increasing carbon fiber content. After the MPTMS treatment, the specific wear rate was decreased. Similar to friction coefficient, M-CF and M-GO increase the bond strength with the PPS matrix which makes the decrement of wear loss. The addition of MPTMS-treated GO to the PPS/CF composite has reduced the wear rate and friction coefficient. The specific wear rate of PPS/20M-CF/5M-GO was comparable to recent results of PPS composites (see Table 3).

Fig. 9 shows the FE-SEM images of the composite surface after the wear test. Each composite shows wear tracks, which were created by balls during the wear test. The surface of wear track shows smoother surface than undamaged surface. The carbon fibers have almost not been damaged because carbon fiber withstands a high temperature of 800 °C as shown in TGA results. The wear tracks are about almost same height as where they were not worn due to the small wear loss after wear test which can be seen that the tribological properties were enhanced by adding MPTMS-treated carbon fiber and GO as shown in Fig. 8(b). In summary, by adding MPTMS-treated carbon fiber and GO to the PPS matrix, the thermal, mechanical, and tribological properties of the composite have been improved.

4. Conclusions

In this study, carbon fiber and GO fillers were treated with MPTMS to increase the bonding strength between the PPS matrix and fillers. The carbon fibers remained stable during the high-temperature treatment and treatment with the chemical solvent; the oxidation process was conducted before the MPTMS treatment. The MPTMS-treated fillers were studied with different methods. The treated and untreated fillers were added to the PPS matrix and melted together with twin-screw melt extrusion; in addition, PPS/CF/GO composites were fabricated with melting injection molding. The MPTMS-treated carbon fiber and GO-containing composite shows improved thermal properties (the thermal conductivity has increased from 0.185 to 0.323 W/m•K) and mechanical properties (the Young's modulus has increased 188% higher than neat PPS, and the tensile strain has been improved). Although the addition of carbon fibers decreased the tensile stress first, in the case of the MPTMS-treated carbon fiber composite, the tensile stress is similar to the tensile stress of neat PPS. This may be due to the increased bonding strength between the PPS and MPTMS-treated fillers. The thermal conductivity of the PPS/20M-CF/5M-GO composite was increased to 0.323 which is 175% greater than neat PPS. After the wear test, the friction coefficient decreased owing to the carbon fibers; in addition, the specific wear rate is approximately 400% better than that of neat PPS. Thus, PPS/CF/GO composites are suitable candidates for heat pumps and interior materials in the automotive industry.

Author statement

Minsu Kim Conceptualization, Investigation, Writing – Original Draft, Data curation, Formal analysis, Methodology, Jooyoung Lee Investigation, Data curation, Formal analysis, Prof. Minhaeng Cho Supervision, Project administration, Methodology, Prof. Jooheon Kim Supervision, Project administration, Funding acquisition.

Declaration of competing interest

The authors declare that they have no known competing financial interests or personal relationships that could have appeared to influence the work reported in this paper.

Acknowledgements

References

[1] P.E. Irving, C. Soutis, Polymer Composites in the Aerospace Industry, Woodhead Publishing, 2019.

[2] A. Iqbal, A. Saeed, A. Ul-Hamid, A review featuring the fundamentals and advancements of polymer/CNT nanocomposite application in aerospace industry, Polym. Bull. 78 (2021) 539–557.

[3] D. Park, H. Ju, J. Kim, Enhanced thermoelectric properties of flexible N-type Ag2Se nanowire/polyvinylidene fluoride composite films synthesized via solution mixing, J. Ind. Eng. Chem. 93 (2021) 333–338.

[4] C. Yang, H. Wei, L. Guan, J. Guo, Y. Wang, X. Yan, X. Zhang, S. Wei, Z. Guo, Polymer nanocomposites for energy storage, energy saving, and anticorrosion, J. Mater. Chem. A 3 (2015) 14929–14941.

[5] S. Kalia, K. Thakur, A. Celli, M.A. Kiechel, C.L. Schauer, Surface modification of plant fibers using environment friendly methods for their application in polymer composites, textile industry and antimicrobial activities: a review, J. Environ. Chem. Eng. 1 (2013) 97–112.

[6] C. Wu, D.T. Chiu, Highly fluorescent semiconducting polymer dots for biology and medicine, Angew. Chem. Int. 52 (2013) 3086–3109.

[7] S.L. Perry, Phase separation: bridging polymer physics and biology, Curr. Opin. Colloid Interface Sci. 39 (2019) 86–97.

[8] J. Holbery, D. Houston, Natural-fiber-reinforced polymer composites in automotive applications, JOM 58 (2006) 80–86.

[9] V. Volpe, S. Lanzillo, G. Affinita, B. Villacci, I. Macchiarolo, R. Pantani, Lightweight high-performance polymer composite for automotive applications, Polymers 11 (2019) 326.

[10] A. Kausar, A review of filled and pristine polycarbonate blends and their applications, J. Plastic Film Sheeting 34 (2018) 60–97.

[11] A. Patil, A. Patel, R. Purohit, An overview of polymeric materials for automotive applications, Mater. Today Proc. 4 (2017) 3807–3815.

[12] C.D. May, R.J. Watling, The development of analytical and interpretational protocols to facilitate the provenance establishment of polycarbonate headlamp lens material, J. Forensic Sci. 56 (2011) S47–S57.

[13] C. Seubert, K. Nietering, M. Nichols, R. Wykoff, S. Bollin, An overview of the scratch resistance of automotive coatings: exterior clearcoats and polycarbonate hardcoats, Coatings 2 (2012) 221–234.

[14] C. Sonsino, E. Moosbrugger, Fatigue design of highly loaded short-glass-fibre reinforced polyamide parts in engine compartments, Int. J. Fatig. 30 (2008) 1279–1288.

[15] H. Oliver-Ortega, F. Julian, F.X. Espinach, Q. Tarrés, M. Ardanuy, P. Mutjé, Research on the use of lignocellulosic fibers reinforced bio-polyamide 11 with composites for automotive parts: car door handle case study, J. Clean. Prod. 226 (2019) 64–73.

[16] D.Q. Dao, J. Luche, T. Rogaume, F. Richard, L. Bustamante-Valencia, S. Ruban, Polyamide 6 and polyurethane used as liner for hydrogen composite cylinder: an estimation of fire behaviours, Fire Technol. 52 (2016) 397–420.

[17] M. Davoodi, S. Sapuan, D. Ahmad, A. Aidy, A. Khalina, M. Jonoobi, Effect of polybutylene terephthalate (PBT) on impact property improvement of hybrid kenaf/glass epoxy composite, Mater. Lett. 67 (2012) 5–7.

[18] I. Panaitescu, T. Koch, V.-M. Archodoulaki, Accelerated aging of a glass fiber/polyurethane composite for automotive applications, Polym. Test. 74 (2019) 245–256.

[19] K. Senthilvel, B. Prabu, Novel carbon black-halloysite nanotube reinforced NBR-PVC hybrid oil seals for automotive applications, Recent Pat. Mater. Sci. 11 (2018) 83–90.

[20] F.M. Al-Oqla, Investigating the mechanical performance deterioration of Mediterranean cellulosic cypress and pine/polyethylene composites, Cellulose 24 (2017) 2523–2530.

[21] J. Sreedharan, A. Jeevanantham, Analysis of shrinkages in ABS injection molding parts for automobile applications, Mater, Today Off.: SAVE Proc. 5 (2018) 12744–12749.

[22] Z. Chen, T. Li, Y. Yang, X. Liu, R. Lv, Mechanical and tribological properties of PA/PPS blends, Wear 257 (2004) 696–707.

[23] T. Canel, İ. Bağlan, T. Sinmazcelik, Mathematical modelling of laser ablation of random oriented short glass fiber reinforced Polyphenylene sulphide (PPS) polymer composite, Opt Laser. Technol. 115 (2019) 481–486.

[24] D. Zhang, H. Qi, F. Zhao, G. Zhang, T. Wang, Q. Wang, Tribological performance of PPS composites under diesel lubrication conditions, Tribol. Int. 115 (2017) 338–347.

[25] A. Jain, J. Somberg, N. Emami, Development and characterization of multi-scale carbon reinforced PPS composites for tribological applications, Lubricants 7 (2019) 34.

[26] B. Vieille, J. Aucher, L. Taleb, Influence of temperature on the behavior of carbon fiber fabrics reinforced PPS laminates, Mater. Sci. Eng., A 517 (2009) 51–60.

[27] N. Forintos, T. Czigany, Multifunctional application of carbon fiber reinforced polymer composites: electrical properties of the reinforcing carbon fibers–A short review, Compos. B Eng. 162 (2019) 331–343.

[28] K. Stoeffler, S. Andjelic, N. Legros, J. Roberge, S.B. Schougaard, Polyphenylene sulfide (PPS) composites reinforced with recycled carbon fiber, Compos. Sci. Technol. 84 (2013) 65–71.

[29] S. Zhou, Q. Zhang, C. Wu, J. Huang, Effect of carbon fiber reinforcement on the mechanical and tribological properties of polyamide6/polyphenylene sulfide composites, Mater. Des. 44 (2013) 493–499.

[30] B. Pan, S. Zhang, W. Li, J. Zhao, J. Liu, Y. Zhang, Y. Zhang, Tribological and mechanical investigation of MC nylon reinforced by modified graphene oxide, Wear 294 (2012) 395–401.

[31] Y.-J. Wan, L.-X. Gong, L.-C. Tang, L.-B. Wu, J.-X. Jiang, Mechanical properties of epoxy composites filled with silane-functionalized graphene oxide, Compos. A: Appl. Sci. Manuf. 64 (2014) 79–89.

[32] W. Lee, J. Lee, P. Reucroft, XPS study of carbon fiber surfaces treated by thermal oxidation in a gas mixture of O2/(O2+ N2), Appl. Surf. Sci. 171 (2001) 136–142.

[33] L. Stobinski, B. Lesiak, A. Malolepszy, M. Mazurkiewicz, B. Mierzwa, J. Zemek, P. Jiricek, I. Bieloshapka, Graphene oxide and reduced graphene oxide studied by the XRD, TEM and electron spectroscopy methods, J. Electron. Spectrosc. Relat. Phenom. 195 (2014) 145–154.

[34] M. Guan, W. Liu, Y. Shao, H. Huang, H. Zhang, Preparation, characterization and adsorption properties studies of 3-(methacryloyloxy) propyltrimethoxysilane modified and polymerized sol–gel mesoporous SBA-15 silica molecular sieves, Microporous Mesoporous Mater. 123 (2009) 193–201.

[35] S.S. Kim, J.E. Park, J. Lee, Properties and antimicrobial efficacy of cellulose fiber coated with silver nanoparticles and 3-mercaptopropyltrimethoxysilane (3-MPTMS), J. Appl. Polym. Sci. 119 (2011) 2261–2267.

[36] D. Semitekolos, A.-F. Trompeta, I. Husarova, T. Man'ko, A. Potapov, O. Romenskaya, Y. Liang, X. Li, M. Giorcelli, H. Dong, Comparative physical–mechanical properties assessment of tailored surface-treated carbon fibres, Materials 13 (2020) 3136.

[37] X.-J. Shen, X.-Q. Pei, Y. Liu, S.-Y. Fu, Tribological performance of carbon nanotube–graphene oxide hybrid/epoxy composites, Compos. B Eng. 57 (2014) 120–125.

[38] S. Pan, H. Shen, L. Zhang, Effect of carbon nanotube on thermal, tribological and mechanical properties of 3D printing polyphenylene sulfide, Addit. Manuf. 47 (2021) 102247.

[39] Y. Shi, S.-T. Zhou, Z.-G. Heng, M. Liang, Y. Wu, Y. Chen, H.-W. Zou, Interlocking structure formed by multiscale carbon fiber–polytetrafluoroethylene fiber hybrid significantly enhances the friction and wear properties of polyphenylene sulfide based composites, Ind. Eng. Chem. Res. 58 (2019) 16541–16551.

[40] W. Luo, Q. Liu, Y. Li, S. Zhou, H. Zou, M. Liang, Enhanced mechanical and tribological properties in polyphenylene sulfide/polytetrafluoroethylene composites reinforced by short carbon fiber, Compos. B Eng. 91 (2016) 579–588.

[41] W. Ren, Y. Yang, J. Yang, H. Duan, G. Zhao, Y. Liu, Multifunctional and corrosion resistant poly (phenylene sulfide)/Ag composites for electromagnetic interference shielding, Chem. Eng. J. 415 (2021) 129052.

[42] Y. Shi, Y. Bai, Y. Lei, H. Zhang, S. Zhou, H. Zou, M. Liang, Y. Chen, Simultaneously enhanced heat dissipation and tribological properties of polyphenylene sulfide-based composites via constructing segregated network structure, J. Mater. Sci. Technol. 99 (2022) 239–250.